

Fume Pyrolysis of Nickel-Containing Silica Sol for the Preparation of a Microporous Ni/SiO_2 Catalyst and a Comparison with Other Nickel-Loading Methods onto Microporous Silica

Takanori Mizushima,* Kenji Nishida, Hironobu Ohkita, and Noriyoshi Kakuta

Department of Materials Science, Toyohashi University of Technology, Hibarigaoka, Tempaku-cho, Toyohashi, Aichi 441-8580

(Received April 9, 2002)

A fume pyrolysis technique using a nickel-containing tetraethoxysilan solution was applied to the preparation of a microporous and highly dispersed Ni/SiO_2 catalyst and compared with nickel-loading onto microporous silica by the conventional impregnation and ion-exchange methods. During impregnation, although the microporous structure remained unaltered, large Ni particles were deposited onto the external surface of the silica particles. Although the ion-exchange method resulted in a high dispersion, the process eroded the silica texture and lowered the pore volume remarkably. In contrast, the fume pyrolysis of a spray of a solution consisting of nickel-incorporated siloxane polymers, prepared through an alkoxide procedure, formed a catalyst which had very small Ni particles in micropores of silica. In spite of the same precursory solution, a simple dryness by evaporation led to pore expansion into the mesopore region and a decrease in the Ni dispersion.

Since the pore structure of solid catalysts is an important factor which strongly influences the physical properties and catalytic performances, many efforts have been made in the synthesis of porosity-controlled materials. The pore design of amorphous metal oxides has been often achieved by the sol-gel method using metal alkoxides.[1–3] For example, Nakanishi et al.[4–7] have applied it to preparation of silica gel with a hierarchical pore structure. They used a spinodal decomposition of an alkoxysilane solution incorporating soluble polymers to build a controlled macroporous network of silica, and further formed well-defined mesopores on the surface without any destruction of the macrostructure by a solvent-exchange treatment.

We also prepared a porous silica by a fume pyrolysis (FP) technique using a silica sol prepared through a sol-gel method, and found that the resulting powder consisted of spherical particles with the porosity deeply depending on the preparation conditions.[8,9] The pore size of the silica collected in water after an instantaneous burning of a spray of a tetraethoxysilan (TEOS) solution could be controlled in the micro-and mesopore regions by adjusting the pyrolysis temperature. Among them, silica obtained at 773 K had pores of about 0.6 nm in diameter, which were expected to cause a molecular sieving effect. In fact, differences in the rate and amount of adsorption were observed between benzene and *o*-xylene. The pore size was also affected by the collection method: the silica formed in the pyrolysis tube heated at 1123 K and then collected with a paper filter had micropores of less than 1.5 nm, whereas the water collection resulted in a pore expansion to 4–5 nm. On the other hand, elevating the viscosity of the precursory solution raised the pore volume and the BET surface area with the pore opening size being kept constant.

The results mentioned above lead to an expectation of the control of catalytic reactions by the pore structure, and hence the loading of catalytic active species into the pores is strongly desired in the next stage of this study. We first attempted to load Ni onto the microporous silica by impregnation (Imp) and ion-exchange (IE) methods in the present work. Furthermore, the fume pyrolysis of a nickel-containing TEOS solution was carried out for a direct synthesis of microporous and a highly dispersed Ni/SiO_2 catalyst and compared with a simple dryness by evaporating the same solution.

Experimental

Catalyst Preparation. The microporous silica employed in this work was prepared by the fume pyrolysis of an aqueous TEOS solution, the details of which were previously reported.[8,9] In short, a solution with a $TEOS/H_2O$ molar ratio of 1/120 was first stirred at 353 K after adjusting to pH 2 with nitric acid. When the viscosity reached 2.0 mPa s through the hydrolysis and polycondensation of the TEOS, the solution was fumed with a supersonic vibrator at 1.5 MHz. The small liquid particles generated were instantaneously solidified in an oxygen stream through a quartz tube heated at 1123 K, followed by collection with paper filter. The obtained silica powder was then dried at 383 K for 12 h and calcined at 773 K for 4 h.

A loading of Ni onto the silica by the conventional impregnation method was carried out using an aqueous $Ni(NO_3)_2{\cdot}6H_2O$ solution. In the ion-exchange procedure, silica powder was immersed in a 0.05 mol/dm^3 $Ni(NO_3)_2$–0.5 mol/dm^3 NH_4COOH solution after adjusting to pH 8 with ammonia water, and was stirred at 353 K for 5 h, followed by a filtration and washing.

On the other hand, the Ni/SiO_2(FP) catalyst was directly obtained by the fume pyrolysis of a nickel-incorporated silica solution, which was prepared according to the alkoxide method.[10,11]

Table 1. Characterization of the SiO_2 and Ni/SiO_2 Catalysts

Catalyst	Ni concentration	Pore size	Pore volume	V_{micro}/V_{total} [a)]	BET surface area
	wt%	nm	cm^3/g	%	m^2/g
SiO_2	—	< 1.5	0.18	84	300
Ni/SiO_2(Imp)	10.0	< 1.5	0.12	82	200
Ni/SiO_2(IE)	5.9	< 1.5, 4.2	0.07	37	34
Ni/SiO_2(FP)	9.7	< 1.5	0.14	65	240
Ni/SiO_2(Evap)	9.7	2.5	0.31	22	520

a) The ratio of the volume of the pores with an opening size of less than 2 nm, V_{micro}, to the total pore volume, V_{total}.

TEOS was fed to a $Ni(NO_3)_2 \cdot 6H_2O$ solution dissolved in ethylene glycol and refluxed at 353 K for 4 h after the addition of nitric acid. Then, 120-times the molar quantity of water to the TEOS was added and stirred until the solution viscosity was raised to be 2.7 mPa s. A part of the thus-prepared solution was subjected to fume pyrolysis under the same conditions as those for the nickel-free silica to obtain solids. The Ni/SiO_2(Evap) catalyst was also produced for a comparison by evaporating the remaining solution to dryness under reduced pressure at 353 K.

All of the obtained catalysts were dried at 383 K for 12 h and calcined at 773 K for 4 h. The nickel amount in the precursory solutions was adjusted so as to be a metal concentration of 10 wt% in the resulting Ni/SiO_2 catalyst when all of the Ni ions were deposited on the silica.

Characterization. The catalyst was examined by a transmission electron microscope (TEM, Hitachi H-800) operated at an accelerating voltage of 200 kV. In order to facilitate an observation of the metal particles, the catalyst was reduced with hydrogen at 773 K for 4 h in advance. A fluorescent X-ray measurement was also carried out to determine the Ni concentration in the catalyst.

The pore size, pore volume, and BET surface area were estimated via the adsorption of nitrogen. After evacuating the sample at 573 K for 1 h, nitrogen adsorption–desorption curves were measured at liquid-nitrogen temperature by using a vacuum system equipped with microcomputer-controlled capacitance manometers and valves. The size and volume of the pores were calculated according to the BJH theory[12] from the desorption data.

A structural analysis of the Ni species was attempted by an X-ray diffractometer (XRD, Rigaku RINT2000) with the Cu-$K\alpha$ radiation. EXAFS was also applied to some of the samples which did not show any XRD peaks. The spectra were measured with a laboratory EXAFS system (Rigaku R-EXAFS 2000) consisting of a strong X-ray generator, a Ge(220) monochromating crystal of the Johansson type, and an ionization chamber and a scintillation counter to detect the incident and transmitted X-rays, respectively.

Furthermore, the Ni species were evaluated through the temperature programmed reduction (TPR) method. The amount of hydrogen consumed for the reduction of the catalyst in a stream of 10% H_2/Ar was determined by a thermal-conductivity detector as a function of the temperature elevating from 293 to 1173 K at a rate of 10 K/min.

Results

Ni Concentration and Catalyst Morphology. The Ni concentration measured by fluorescent X-ray spectroscopy is summarized in Table 1. Although the Ni amount in Cat(IE) was only about 60% of that in the precursory solution, the designed concentration was achieved by other preparation procedures.

The TEM observation elucidated that the nickel-free silica prepared by the fume pyrolysis method consisted of spherical particles of 0.5–3 μm in diameter; the size was rarely changed after the nickel-loading processes. Typical TEM photographs of the relatively small particles among the Ni/SiO_2 catalysts as well as the raw silica are shown in Fig. 1.

It is evident from Fig. 1b that Cat(Imp) contained some Ni particles of 20–100 nm on the external surface of the silica. Unfortunately, a very low transmittance of electrons prevented the Ni species inside the silica particles from being detected. On the other hand, no Ni particle was found in Fig. 1c, indicating that a high dispersion of the Ni was obtained by the ion-exchange method. The outline of the silica particle, however, is blurred compared with Fig. 1a. This implies that the process caused a partial dissolution of the silica surface.

Doping Ni into the TEOS solution by the alkoxide method did not affect the shape and size of the particles; the Ni/SiO_2(FP) catalyst contained spherical particles of 0.5–3 μm. Figure 1d is a TEM photograph of a relatively small one. Because Ni crystallites were not found on the silica, very small Ni species were presumed to be in the pores. An erosion of the silica surface was not observed. In contrast, Cat(Evap) prepared from the same precursory solution as that for Cat(FP) was composed of Ni particles with a diameter of 4–12 nm on scale-like pieces of silica, as is shown in Fig. 1e.

Pore Structure. Figure 2 shows nitrogen adsorption-desorption isotherms determined at liquid-nitrogen temperature. The pore-size distributions and the porosity parameters calculated from the data are also given in Fig. 3 and Table 1, respectively. The adsorption profile of the silica before the nickel-loading (Fig. 2a) belonged to Type I in the IUPAC classification, indicating that the silica was microporous. The pore size was estimated to be less than 1.5 nm, below which the BJH theory can not be applied. The ratio of the volume of the micropores to the total pore volume, V_{micro}/V_{total}, was 84%.

After loading the Ni onto the silica by the impregnation method, although the saturated adsorption amount of nitrogen decreased by 33%, the shape of the isotherm was scarcely affected. In addition, the ratio V_{micro}/V_{total} was almost the same as that of the nickel-free silica; therefore the microporous texture remained after the process. By assuming that NiO crystallites with the same density as that of the bulk, 6.96 g/cm^3, were formed in the calcined catalyst, 1 g of the 10 wt% Ni/SiO_2 catalyst was calculated to contain 0.88 g of the silica, which had a total pore volume of 0.16 cm^3; 0.12 g of the NiO which corresponded to a volume of 0.017 cm^3. Although the TEM photograph (Fig. 1b) reveals the existence of Ni particles outside the

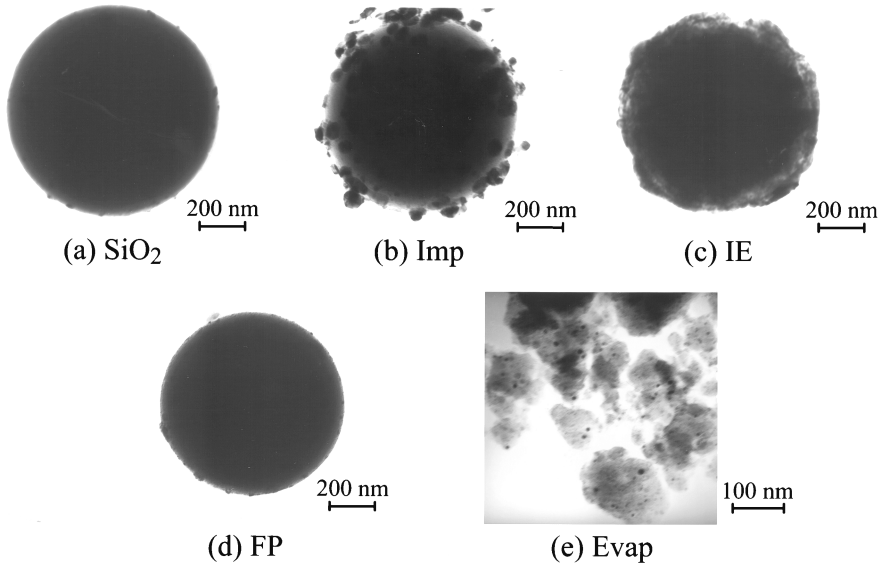

Fig. 1. TEM photographs of (b–e) the reduced Ni/SiO_2 catalysts and (a) the Ni-free SiO_2.

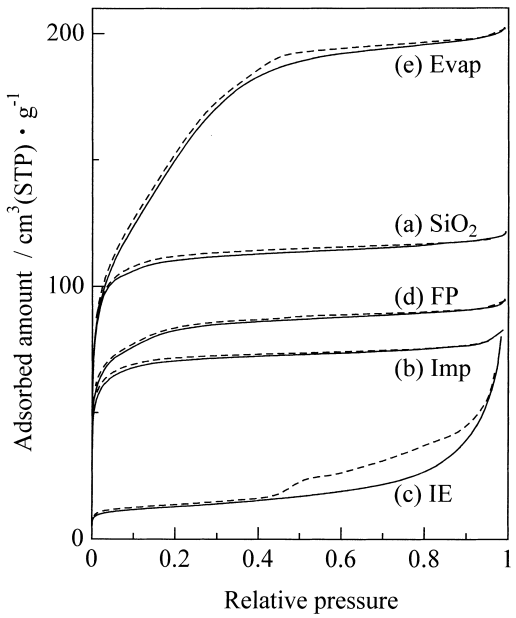

Fig. 2. Nitrogen adsorption-desorption isotherms of (b–e) the Ni/SiO_2 catalysts and (a) the Ni-free SiO_2.

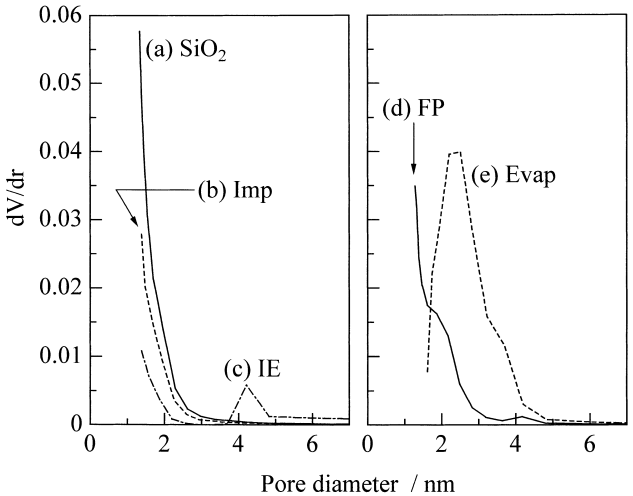

Fig. 3. Pore size distributions of (b–e) the Ni/SiO_2 catalysts and (a) the Ni-free SiO_2.

silica, an assumption that all of the NiO crystallites are in the pores leads to an estimation for the pore volume to be 0.16–0.017 $\approx$ 0.14 cm^3/g. The observed value, 0.12 cm^3/g, was still smaller than this value, suggesting that some of the Ni particles were deposited in the micropores and/or at the pore openings to block the penetration of nitrogen molecules.

On the other hand, Cat(IE) showed quite a different curve from those of the silica and Cat(Imp): (1) the profile was transformed to Type IV, (2) the amount adsorbed remarkably decreased, and (3) a hysteresis appeared. The BJH analysis revealed the formation of mesopores with a diameter of 4.2 nm and a decrease of 61% in the pore volume. This supports the TEM result that the ion-exchange process gave rise to the dissolution and erosion of the silica.

For Cat(FP), although the amount adsorbed was smaller, the adsorption profile was the same type as that of the nickel-free silica, suggesting that the catalyst was microporous. In contrast, a distinct type of adsorption was observed for Cat(Evap); the adsorbed amount continued to gradually increase after a relative pressure of 0.05, at which the micropores were filled with nitrogen. It was found from the BJH analysis that Cat(Evap) had mesopores of about 2.5 nm with a wide distribution, as is shown in Fig. 3e. These results lead to a conclusion that the pore structure deeply depended on the solidification process of the nickel-containing silica solution.

XRD. XRD patterns of the Ni/SiO_2 catalysts before and after reduction are illustrated in Fig. 4. The broad hump observed around 23 degrees for all of the samples was attributable to the amorphous silica.

The diffraction peaks at 37.3, 43.3, and 62.9 degrees in Fig. 4a were assigned to the reflections from the (101), (012), and (110) planes of NiO, respectively, indicating the formation of

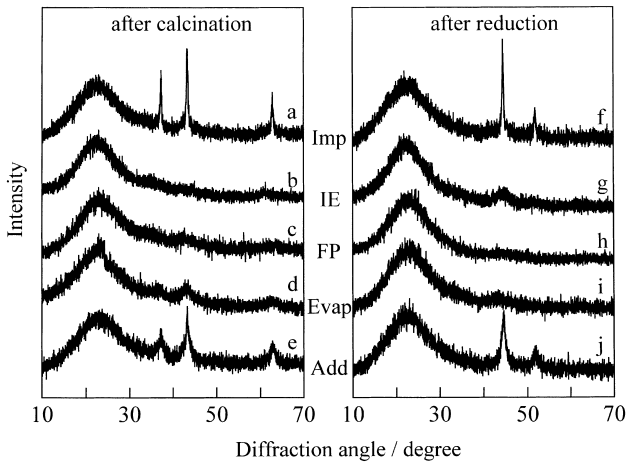

Fig. 4. XRD patterns of the Ni/SiO_2 catalysts after (a–e) calcination and (f–j) reduction.

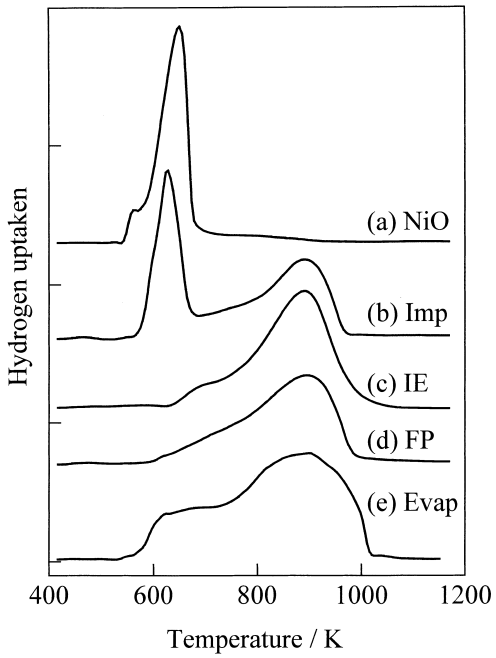

Fig. 5. TPR profiles of (b–e) the Ni/SiO_2 catalysts and (a) unsupported NiO powder.

bulky NiO crystals in Cat(Imp) after calcination. Reducing the sample with hydrogen at 773 K for 4 h resulted in a disappearance of the NiO peaks and the appearance of two peaks at 44.5 and 51.9 degrees in Fig. 4f. These peaks corresponded to the Ni(111) and Ni(200) reflections, respectively; therefore the NiO particles were reduced to metals. Because no bulks which give intense XRD peaks can be in the micropores, it is concluded that the peaks seen in Figs. 4a and 4f are attributed to the large Ni particles observed on the external surface of the silica by TEM.

On the other hand, there is no diffraction peak in the XRD of Cat(IE) after calcination (Fig. 4b), and hence the Ni species were supposed to be highly dispersed. The small hump at around 45 degrees in Fig. 4g resulted from small metal clusters, implying a small degree of aggregation of the Ni species in the reduction step. The Ni/SiO_2 catalysts prepared through the alkoxide technique, Cat(FP) and Cat(Evap), also had a high Ni dispersion, as is evident from Figs. 4c, 4d, 4h, and 4i. However, very small and broad protrusions observed at the same angles as those of crystalline NiO in Fig. 4d suggest that the Ni ions had a tendency to be aggregated in Cat(Evap) compared with Cat(FP).

A feature of the alkoxide method is that Ni–O–Si bonds formed in the precursory solution prevent the Ni from sintering. In order to confirm this effect in Cat(Evap), we also prepared a 10 wt% Ni/SiO_2(Add) catalyst by evaporating a mixed solution of nickel(II) nitrate and silica sol. Because $Ni(NO_3)_2 \cdot 6H_2O$ was added after the polymerization of TEOS, the Ni–O–Si bonds in Cat(Add) were expected to be less than those in Cat(Evap). The XRD results are given in Figs. 4e and 4j. Apparent diffraction peaks due to NiO after calcination and due to Ni metal after the reduction mean the formation of large crystallites of Ni in comparison with Cat(Evap). This clearly indicates that the Ni–O–Si bonds were established in Cat(Evap) to inhibit a sintering of the Ni.

TPR. Figure 5 shows TPR profiles of the calcined catalysts as well as the unsupported NiO powder as a reference. It is evident from the figure that there were two kinds of Ni species in the silica-supported catalysts: one of them was reduced under 700 K, whereas the other required a higher temperature than 800 K for reduction. A low-temperature peak was also observed for the unsupported NiO powder, and hence it was assigned to a reduction of Ni^{2+} ions to Ni^0 atoms in crystalline NiO particles without a significant chemical bond with the support. In contrast, the high-temperature peak was presumed to be due to the fine Ni species which had interactions with the silica.

The TPR of Cat(Imp) clearly demonstrated the formation of less reducible species in addition to the large NiO crystallites. The amount of H_2 consumed at the low-temperature peak (500–700 K) was about 45% of the total. Cat(Evap) also contained both species, but the ratio of the low-temperature peak decreased to about 15% and the high-temperature peak simultaneously grew. On the other hand, Cat(IE) and Cat(FP) were found to consist of only the less-reducible species. These results are consistent with those observed by TEM and XRD.

EXAFS. Since no apparent XRD peak was detected for Cat(FP), we tried a structural analysis of the Ni by means of EXAFS spectroscopy. Figures 6a-c illustrate a change in the Fourier transformation of the k^3-weighed Ni *K*-EXAFS of Cat(FP) in the calcination step. The results of Cat(Evap) and unsupported NiO powder are also given in Figs. 6d–f and g, respectively. It should be noted that the peaks in the figures are located at the shorter interatomic distances than the real values because the phase correction was not made in the Fourier transformation.

For Cat(Evap) before calcination, only one peak due to Ni–O bonds was observed at 0.16 nm in Fig. 6d. Heating the sample at 473 K resulted in the appearance of an additional peak at 0.26 nm in Fig. 6e. This peak further grew by calcination at 773 K (Fig. 6f) and its intensity ultimately was comparable to that of the nearest Ni–Ni peak in Fig. 6g.

The EXAFS-Fourier transformation of Cat(FP) before calcination (Fig. 6a) showed a very small peak of the second near-

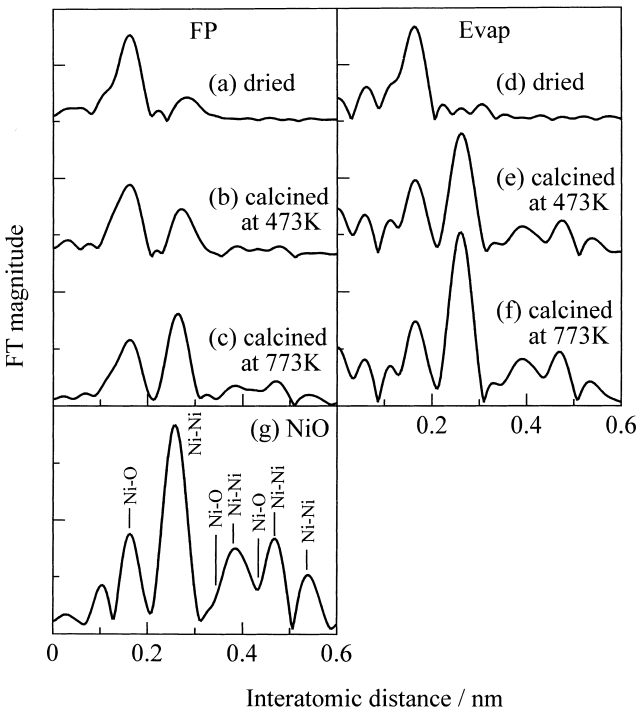

Fig. 6. Fourier transforms of EXAFS spectra of the Ni/SiO_2 catalysts prepared by (a–c) FP and (d–f) Evap, and (g) unsupported NiO powder.

est coordinations in addition to the Ni–O peak. Its maximum was located at 0.28 nm, which was 0.02 nm longer than that of the nearest Ni–Ni peak in the NiO. This peak became more intense and was shifted to shorter distances as the calcination temperature was raised. However, the final intensity after calcination at 773 K did not arrive at half of the second nearest peak in Fig. 6g and the interatomic distance was slightly longer. From these results, it is anticipated that Cat(FP) had a very high dispersion and the local structure around the Ni was slightly different from that in crystalline NiO.

Discussion

Three techniques (impregnation, ion-exchange, and fume pyrolysis) were tried to prepare a microporous and highly dispersed Ni/SiO_2 catalyst in the present work. As a result, the Ni dispersion by the impregnation method was very poor and the ion-exchange process destroyed the microporous structure of the silica. The intended material was obtained by fume pyrolysis of the nickel-containing TEOS solution; the fine Ni species were deposited in pores with a diameter of less than 1.5 nm. Accordingly, the porosity and structure of the Ni/SiO_2(FP) catalyst will hereinafter be discussed by comparing with Cat(Evap), which was prepared from the same precursory solution.

Porosity of the Ni/SiO_2(FP) Catalyst. In the alkoxide method, the nickel glycoxide formed from nickel(II) nitrate and ethylene glycol reacts with TEOS to make Ni–O–Si bonds, as shown in Scheme 1.[10,11] The Ni compounds produced and the excess TEOS's are then hydrolyzed and polycondensed to build a silicate network incorporating the Ni ions, resulting in a gradual increase in the solution viscosity. The reaction is allowed to continue until the sol transforms into a gel in the ordinary alkoxide method, but was suspended at a relatively low viscosity to be subjected to the fume pyrolysis in this work; therefore, the networked clusters of the silicates employed were considered to be immature and small compared with those obtained after gelation. It seems reasonable to see that the pores of the resultant catalyst are apertures retained between the silicate clusters after drying and calcination processes, and are enlarged with the size of the silicate clusters. In the preparation of Cat(Evap), a long-time heating for evaporation of the sol probably caused a further polymerization to develop the silicate network, leading to an expansion of the pores. On the other hand, since the fume pyrolysis process was completed for an instant, the silicates likely escaped from an additional polycondensation and were kept to be small during solidification. This brought about a close aggregation of the silicate clusters and the formation of micropores.

Table 1 indicates that the pore volume of the nickel-free silica prepared from the solution with a viscosity of 2.0 mPa s was larger than that of the Ni/SiO_2(FP) catalyst prepared from a 2.7 mPa s solution. However, this conflicts with the fact reported in previous papers,[8,9] that an increasing viscosity led to an increase in the pore volume. The ratio V_{micro}/V_{total} for Cat(FP) was also smaller than that for pure silica. These results suggest some subtle distinctions between the microporous structures of both. We attribute this to a difference between the shapes of the silicate polymers produced in the precursory solutions with and without Ni. A small-angle X-ray scattering study on the fractal geometry of the silica condensation polymers by Schaefer et al.[13] revealed the formation of randomly branched analogs of self-avoiding linear chains from metal-free TEOS. On the other hand, Hayashi et al.[14] reported that nickel-doping by the alkoxide method led to a tendency for the silicate polymers to be linear or less branched. Such a morphological factor of the precursory polymers probably affected their aggregation and sintering during fume pyrolysis, making a difference between the microporous properties of the pure silica and the Ni/SiO_2(FP) catalyst.

Structure and Dispersion of the Ni Species in the Ni/SiO_2(FP) Catalyst. As mentioned above, a feature of the alkoxide method is the creation of Ni–O–Si bonds in solution. This was confirmed from the EXAFS of dried TEOS gel incorporating Ni by Tohji et al.,[11] who detected the second nearest peak in addition to the nearest Ni–O peak and assigned it to the Ni–(O)–Si coordination with an interatomic distance of 0.330 nm. Unfortunately, it can not be observed in Fig. 6d, but the XRD result that Cat(Evap) had a higher resistance to the Ni sintering than Cat(Add) clearly reveals that the Ni–O–Si bonds were established in the dried Ni/SiO_2(Evap) catalyst.

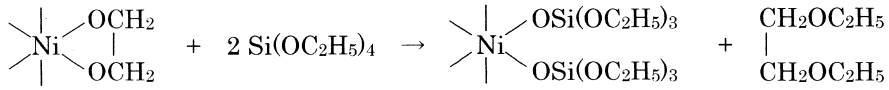

Scheme 1.

An absence of the Ni–(O)–Si peak in Fig. 6d is presumably attributable to differences in the preparation conditions. For the hydrolysis and polycondensation of the Ni-TEOS sol, Tohji et al.[11] used H_2O in a ratio of 4 : 1 by volume to the TEOS, which corresponded to a H_2O/TEOS molar ratio of about 50. Furthermore, the final catalyst was obtained after the sol was transformed into a gel where the silicate network was developed all over. In contrast, a large excess of water (H_2O/TEOS = 120) was employed, and the polymerization was stopped before the gelation in this work. These differences may cause a decrease in the number of the Ni–O–Si bonds, making them undetectable by EXAFS spectroscopy. A lowering of the crystallinity is also supposed to be one of the causes; an uneven bond angle of the Ni–O–Si raised the nonuniformity of the interatomic distance between the Ni and Si ions, resulting in a lack of the Ni–(O)–Si peak.

On the other hand, the second-nearest peak was observed for Cat(FP) even after drying, as is shown in Fig. 6a. There are two possibilities, Ni–(O)–Si and Ni–(O)–Ni coordinations, for this peak, but it is hard to distinguish between them because the peak is very small and broad.

For that reason, we tried to describe it through a comparison between the EXAFS data of Cat(FP) and Cat(Evap) after calcination at 773 K. The structural parameters for the first and second nearest peaks in Figs. 6c and 6f were estimated by a curve-fitting analysis with the phase shift and backscattering function extracted from the first and second nearest peaks in Fig. 6g. Because an adequate reference material to obtain the scattering parameters of Ni–(O)–Si was not available, the second-nearest peaks were analyzed under an assumption that they consisted of only Ni–(O)–Ni coordinations; that is, all of the Ni ions existed as NiO.

The interatomic distances of the Ni–O and Ni–(O)–Ni in Cat(Evap) were calculated to be 0.210 and 0.297 nm, respectively. These were identical with those in the NiO crystal. The coordination numbers of 6.2 for the Ni–O and 12.5 for Ni–(O)–Ni were also comparable to 6 and 12 in NiO, respectively; therefore, crystalline NiO particles were considered to be formed in Cat(Evap) after calcination at 773 K.

The coordination number of the Ni–O in Cat(FP) was identical to that in the NiO crystal, but its bond length was shorter by 0.003 nm. The coordination number of the second shell was estimated to be 7.4. This is much smaller than those in Cat(Evap) and the NiO, suggesting that the particles were very small. Its interatomic distance was 0.300 nm, which was 0.003 nm longer than that in the NiO. It is therefore presumed that the local environment around the Ni in Cat(FP) was slightly different from that in the crystalline NiO.

Similar tendencies for the Ni–O bond length to be shortened and for the interatomic distance of the second nearest coordinations to be lengthened were reported by Clause et al.[15,16] for Ni/SiO_2 catalysts prepared by the deposition-precipitation and ion-exchange methods. They found that the second coordination shell around the Ni contained Ni and Si ions, which led to the conclusion that a nickel silicate was formed on the support.

The surface nickel silicate was also identified by TPR. van de Loosdrecht et al.[17] observed two reduction steps for a 20 wt% Ni/SiO_2 catalyst, and assigned the high-temperature peak to a reduction of nickel hydrosilicate. Similar conclusions were reported by Mile et al.[18] and Hadjiivanov et al.[19]

An agreement of our EXAFS and TPR results with the above reports suggests the formation of nickel silicates in Cat(FP); therefore the second-nearest peaks in Figs. 6a-c are attributed to not only Ni, but also Si ions. Although the nickel silicates were also supposed to be formed in Cat(Evap), it was revealed by the EXAFS and TPR measurements that the Ni ions tended to aggregate and form large NiO particles compared with Cat(FP). This was probably contributed by the difference in the pore structures; the Ni species could easily move and aggregate to form large particles in the mesopores of Cat(Evap), whereas a spatial restriction in the micropores of Cat(FP) greatly inhibited the growth of particles, and led to a high dispersion.

References

1 C. G. Guizard, A. C. Julbe, and A. Ayral, *J. Mater. Chem.*, **9**, 55 (1999).

2 J. J. E. Moreau and M. W. C. Man, *Coord. Chem. Rev.*, **178**, 1073 (1998).

3 C. J. Brinker, D. M. Smith, R. Deshpande, P. M. Davis, S. Hietala, G. C. Frye, C. S. Ashley, and R. A. Assink, *Catal. Today*, **14**, 155 (1992).

4 K. Nakanishi, R. Takahashi, and N. Soga, *J. Non-Cryst. Solids*, **147-148**, 291 (1992).

5 K. Nakanishi, *J. Porous Mater.*, **4**, 67 (1997).

6 K. Nakanishi, T. Nagakane, and N. Soga, *J. Porous Mater.*, **5**, 103 (1998).

7 K. Nakanishi, R. Takahashi, T. Nagakane, K. Kitayama, N. Koheiya, H. Shikata, and N. Soga, *J. Sol.-Gel Sci. Tech.*, **17**, 191 (2000).

8 N. Kakuta, T. Tanabe, K. Nishida, T. Mizushima, and A. Ueno, Prep. Catal. VI Proc. Int. Symp. 6th, 1944: Abst. in *Stud. Surf. Sci. Catal.*, **91**, 319 (1995).

9 T. Mizushima, T. Tanabe, K. Nishida, N. Kakuta, and A. Ueno, *J. Catal.*, **168**, 121 (1997).

10 A. Ueno, H. Suzuki, and Y. Kotera, *J. Chem. Soc., Faraday Trans. 1*, **79**, 127 (1983).

11 K. Tohji, Y. Udagawa, S. Tanabe, and A. Ueno, *J. Am. Chem. Soc.*, **106**, 612 (1984).

12 E. P. Barrett, L. G. Joyner, and P. P. Halenda, *J. Am. Chem. Soc.*, **73**, 373 (1951).

13 D. W. Schaefer, and K. D. Keefer, *Phys. Rev. Lett.*, **53**, 1383 (1984).

14 H. Hayashi, K. Tohji, Y. Udagawa, and A. Ueno, *Bull. Chem. Soc. Jpn.*, **66**, 1024 (1993).

15 O. Clause, L. Bonneviot, and M. Che, *J. Catal.*, **138**, 195 (1992).

16 O. Clause, L. Bonneviot, M. Che, and H. Dexpert, *J. Catal.*, **130**, 21(1991).

17 J. van de Loosdrecht, A. M. van der Kraan, A. J. van Dillen, and J. W. Geus, *J. Catal.*, **170**, 217 (1997).

18 B. Mile, D. Stirling, M. A. Zammitt, A. Lovell, and M. Webb, *J. Catal.*, **114**, 217 (1988).

19 K. Hadjiivanov, M. Mihaylov, D. Klissurski, P. Stefanov, N. Abadjieva, E. Vassileva, and L. Mintchev, *J. Catal.*, **185**, 314 (1999).